



Published in final edited form as:

*Electrophoresis*. 2009 September ; 30(18): 3289–3300. doi:10.1002/elps.200900141.

## Highly Efficient Capture and Enumeration of Low Abundance Prostate Cancer Cells Using Prostate-Specific Membrane Antigen Aptamers Immobilized to a Polymeric Microfluidic Device

Udara Dharmasiri, Subramanian Balamurugan, André A. Adams, Paul I. Okagbare, Annie Obubuafo, and Steven A. Soper\*

Department of Chemistry and Center for BioModular Multi-Scale Systems, Louisiana State University, Baton Rouge, Louisiana 70803

### Abstract

Prostate tumor cells over-express a prostate specific membrane antigen (PSMA) that can be used as a marker to select these cells from highly heterogeneous clinical samples, even when found in low abundance. Antibodies and aptamers have been developed that specifically bind to PSMA. In this study, anti-PSMA aptamers were immobilized onto the surface of a capture bed poised within a poly(methyl methacrylate), PMMA, microchip, which was fabricated into a high throughput micro-sampling unit (HTMSU) used for the selective isolation of rare circulating prostate tumor cells resident in a peripheral blood matrix. The HTMSU capture bed consisted of 51 ultra-high aspect ratio parallel curvilinear channels with a width similar to the prostate cancer cell dimensions. The surface density of the PSMA-specific aptamers on a UV-modified PMMA microfluidic capture bed surface was determined to be  $8.4 \times 10^{12}$  molecules/cm<sup>2</sup>. Using a linear velocity for optimal cell capture in the aptamer-tethered HTMSU (2.5 mm/s), a recovery of 90% of LNCaP cells (prostate cancer cell line; used as a model in this example) was found. Due to the low abundance of these cells, the input volume required was 1 mL and this could be processed in approximately 29 min using an optimized linear flow rate of 2.5 mm/s. Captured cells were subsequently released intact from the affinity surface using 0.25% (w/v) trypsin followed by counting individual cells using a contact conductivity sensor integrated into the HTMSU that provided high detection and sampling efficiency (~100%) and did not require staining of the cells for enumeration.

### Keywords

Circulating tumor cells; Prostate specific membrane antigen; Anti-PSMA aptamer; Polymer microfluidics; Conductivity sensor

### INTRODUCTION

Prostate cancer is the most common non-cutaneous malignancy, accounting for 9% of all male cancer-related deaths in the United States; there is a 1 in 6 probability of men in the US developing prostate cancer.<sup>1, 2</sup> In 2007, approximately 220,000 new cases of prostate cancer were recorded and 27,050 prostate cancer-related deaths occurred in the US alone.<sup>3</sup> For more than a decade, determinations of prostate specific antigen (PSA) levels in human serum followed by digital rectal examination have been the predominate diagnostic methods

\*Corresponding author, Phone 225 578 1527, Fax 225 578 3458, chsoper@lsu.edu.

for prostate cancer screening.<sup>4</sup> Men with an abnormal digital rectal examination, as evidenced by the existence of pollups, or elevated prostate specific antigen levels are typically referred for biopsy to assess the presence of prostate cancer. The five region prostate biopsy technique is typically utilized in conjunction with a sextant biopsy.<sup>5</sup> Using these rather invasive diagnostic strategies, up to 30% of prostate cancers are still undiagnosed.<sup>6</sup> Unfortunately, certain medications (e.g. Finasteride), ejaculation, and prostate manipulation (e.g. catheterization, prostate massage) can alter PSA levels and as such, the determination of PSA levels in clinical settings remains controversial.<sup>4</sup>

Mortalities associated with malignant tumors are primarily due to metastasis, which results from the invasion of tissues and organs distant from the primary tumor.<sup>7</sup> The early detection of metastasis is a critical factor for determining the probability of survival for many cancers.<sup>8</sup> At present, reports have noted that circulating tumor cells (CTCs) can be present in peripheral blood for many adenocarcinomas prior to detection of the primary tumor via conventional screening modalities.<sup>9</sup> Therefore, elucidating the presence and number of CTCs in peripheral blood is emerging as an effective tool for risk determination, screening, differential diagnosis and prognosis, disease recurrence, and prediction of specific benefits from particular therapies for the management of cancer-related diseases.<sup>10</sup>

CTCs are an extremely rare component within human blood ( $\sim 10^1$  per mL of whole blood) with the majority cellular components being erythrocytes ( $\sim 10^9$  per mL of whole blood) and leukocytes ( $\sim 10^6$  per mL of whole blood).<sup>11</sup> To discriminate CTCs from these highly abundant species, morphological or chemical differences between the target CTCs and normal hematopoietic components have been exploited,<sup>12</sup> but typically provide low recovery and/or purity.

Disseminated prostate tumor cells can infiltrate the bone marrow, peripheral blood, lymph nodes, stomach, or the penis and the question becomes; can these disseminated tumor cells be used as a clinical marker for prostate cancer staging? Certain cell lines derived from prostate cancers can be used as model systems for the design and evaluation of new assays directed toward prostate cancer using for example CTCs as the diagnostic marker. These cell lines are categorized as to their final metastatic destination, such as bone metastasis – PC3, lymph node metastasis – LNCaP, and those localized to prostate – 22Rv1.<sup>13</sup> Lymph node-based metastasis occur in the very early stages of prostate cancer where high cure rates abound, whereas bone metastasis typically occur in the advanced stages of this disease and is accompanied by significantly reduced quality of life.<sup>14</sup> It has been hypothesized that tumor cells released from a primary tumor site into peripheral blood can be correlated with patient survival or other indicators, such as the presence of regional lymph node metastases. But the use of CTCs as a diagnostic marker is unclear due to the lack of efficient tools for their isolation and enumeration.<sup>15</sup> Therefore, the development of highly efficient CTC isolation and detection systems to search peripheral blood for LNCaP-type cells can potentially generate an effective diagnostic/prognostic tool for prostate cancer.

LNCaP-like cells typically possess a high expression level of the integral membrane protein, prostate-specific membrane antigen (PSMA). PSMA is a homodimeric type II transmembrane glycoprotein consisting of 750 amino acids having a molecular weight of 100 kDa,<sup>16</sup> making PSMA an excellent candidate for tracking LNCaP-type cells to diagnose prostate cancer or to monitor its progression and/or therapeutic response to treatment.<sup>17–19</sup>

Due to the low abundance nature of CTCs in peripheral blood with respect to erythrocytes and leukocytes, the efficiency of CTC isolation is basically characterized by throughput, recovery and purity.<sup>20</sup> Until now, different techniques such as flow assisted cell sorting and immunomagnetic selection have been employed for the isolation of rare cells from complex

clinical samples and are typically fraught with the limitation of choosing between high purity with poor recovery or high recovery with low purity.<sup>21, 22</sup>

While microfluidic systems are emerging as effective tools for biomedical research and diagnostics having such advantages as low reagent consumption, short analysis times and process integration,<sup>22</sup> they are fraught with some limitations, for example the inability to exhaustively sample large input volumes required to search for extremely rare events, such as CTCs in peripheral blood. Two recent examples have appeared in which rare cellular events were accumulated from clinical samples using a microfluidic platform. Nagrath *et al.* described an immunoaffinity approach in which anti-EpCAM (epithelial cell adhesion molecules) antibodies were affixed to micropillars poised within a microfluidic chip capable of extracting CTCs from peripheral whole blood samples with ~50% purity.<sup>11</sup> A polymer-based high throughput microfluidic system was described by Adams *et al.*, in which EpCAM-specific monoclonal antibodies were tethered to parallelized high aspect ratio microchannels that were employed to isolate breast cancer cells (MCF-7) from whole blood demonstrating a recovery of 97% and nearly 100% purity.<sup>20</sup> A compelling attribute of this microfluidic device was its ability to specifically enumerate the CTCs on-chip using an integrated conductivity sensor, which demonstrated a single-cell detection efficiency of 100% without requiring cell labeling.<sup>20</sup>

Though various techniques have been applied to isolate and characterize CTCs, many of them share a similar principle, they use antibody-based selection with integral membrane protein antigens. Application of this molecular recognition strategy for CTC detection is limited by the availability and specificity of antibodies directed against the necessary biomarkers, such as membrane proteins found on different tumor cells.<sup>9</sup> In addition, most of these cell selection tools require surface immobilization of an antibody, which can result in reduced cell recoveries or adhesion strength between the cell and the surface-tethered antibody due to the stochastic nature of the immobilization chemistry.

Aptamers, single-stranded nucleic acid oligomers, possess highly specific recognition affinities to molecular targets through interactions other than classical Watson-Crick base pairing.<sup>23</sup> Compared to antibodies, aptamers have lower molecular weights, demonstrate faster tissue penetration, remain stable during long-term storage, sustain reversible denaturation, low toxicity, and can be produced against targets, such as membrane proteins, using highly automated technologies (i.e., SELEX).<sup>24</sup> In addition, a wealth of literature exists on the immobilization of aptamer recognition elements to solid supports, such as glass,<sup>25</sup> polymers<sup>26</sup> and gold.<sup>26</sup> Additionally, the immobilization chemistry is highly oriented with end-point attachment occurring exclusively through the 5' or 3' end of the aptamer, which bears a functional group, such as a primary amine. These advantages make aptamers highly desirable as potential molecular probes for diagnostics.<sup>27</sup>

Many aptamers have been developed to target the extracellular domains of integral membrane proteins that are over-expressed on cancer cells.<sup>28</sup> Lupold *et al.* first reported RNA aptamers directed against the tumor-associated PSMA membrane antigen and the first application of RNA aptamers that targeted LNCaP cells via the PSMA biomarker. The affinity of this aptamer for PSMA was quantified and suggested that the aptamer identified a unique extracellular domain of PSMA.<sup>29</sup>

Herein, we report on the use of PSMA-specific aptamers tethered to a high throughput micro-sampling unit (HTMSU) with an integrated conductivity sensor employed for the highly efficient isolation and enumeration of rare circulating prostate tumor cells (LNCaP used as a model in these studies) from whole blood without the need for pre-processing of the blood prior to introduction into the microfluidic device nor staining of the CTCs for

enumeration. Nuclease stabilized and *in vitro* generated RNA aptamers were immobilized onto UV-modified curvilinear capture channels comprising the capture bed contained within the microfluidic device using carbodiimide coupling chemistry and the appropriate linker structure to enhance the accessibility of the surface-bound aptamer to the solution-borne cells.<sup>30</sup> The linear velocity of sample introduction into the device was optimized in order to achieve high CTC recovery from blood. After selection and isolation, the captured cells could be released from the capture surface via enzymatic digestion of the extra-cellular domain of PSMA using trypsin for subsequent conductivity enumeration.<sup>20</sup> Recently, Phillips *et al.* has reported on the use of aptamers decorating PDMS microchannel walls for the selection of T-cell acute lymphocytic leukemia cells seeded in an aqueous buffer that was also loaded with a non-cancerous cell line.<sup>31</sup> Unfortunately, this work did not use whole blood as the input sample, which contains extremely high levels of interfering cells and the cell concentration was much higher ( $\sim 1 \times 10^6$  cells/mL) than typically encountered for CTCs found in clinical samples ( $\sim 10$  cells/mL). The results reported here used whole blood as the input with CTC concentrations as small as 10 cells mL<sup>-1</sup>.

## EXPERIMENTAL SECTION

### Buffers and reagents

Poly(methyl methacrylate), PMMA, was used as the HTMSU substrate and cover plate (0.5 mm thickness) and were purchased from Good Fellow (Berwyn, PA). Platinum wires for the conductivity sensor were purchased from Alfa Aesar (Boston, MA). Polyimide-coated fused silica capillaries were purchased from Polymicro Technologies (Phoenix, AZ). Chemicals used for the PMMA surface cleaning and modification included reagent grade isopropyl alcohol, 1-ethyl-3-[3-dimethylaminopropyl] carbodiimide hydrochloride (EDC), N-hydroxysuccinimide (NHS), fetal bovine serum (FBS) and 2-(4-morpholino)-ethane sulfonic acid (MES) and these were purchased from Sigma-Aldrich (St. Louis, MO). The nuclease-resistant RNA aptamer, (NH<sub>2</sub>-(CH<sub>2</sub>)<sub>6</sub>-(OCH<sub>2</sub>CH<sub>2</sub>)<sub>6</sub>-(ACCAAGACCUGACUUCUAACUAAGUCUACGUUCC), was obtained from Eurogentec (San Diego, CA). Random sequence oligonucleotides were obtained from Integrated DNA Technologies (Coralville, IA). Monoclonal anti-EpCAM antibody was obtained from R&D Systems Inc., (Minneapolis, MN). The LNCaP (prostate cancer cell line), MCF-7 (breast cancer cell line), growth media, HEPES buffer, phosphate buffered saline (PBS) and trypsin were all purchased from American Type Culture Collection (Manassas, VA). Citrated rabbit blood was purchased from Colorado Serum Company (Denver, CO). Tris-Glycine buffer was obtained from Bio Rad Laboratories (Hercules, CA). All solutions were prepared in nuclease free water, purchased from Invitrogen Corporation (Carlsbad, CA). Nuclease free microfuge tubes were purchased from Ambion Inc. (Foster City, CA) and were used for preparation and storage of all samples and reagents. A fluorescein derivative, PKH67, which contained a lipophilic membrane linker for cell staining, was purchased from Sigma-Aldrich (St. Louis, MO).

### Cell suspensions

LNCaP and MCF-7 cells were cultured to 80% confluence in Dulbecco's Modified Eagle's Medium supplemented with high glucose containing 1.5 g/L sodium bicarbonate (NaHCO<sub>3</sub>), 15 mM HEPES buffer, and 10% FBS. A 0.25% trypsin solution was prepared in 150 mM PBS and used to harvest the LNCaP and MCF-7 cells from the culturing plate.

LNCaP and MCF-7 cells were stained with PKH67 for microscopic visualization experiments using fluorescence. A modified protocol for cell staining was implemented whereby the dye concentration was increased 2-fold resulting in more evenly distributed fluorescent labels over the cell's periphery. Cell counts for seeding experiments into whole

blood were determined by counting three aliquots of cells in succession using a hemacytometer. The cell count accuracy was  $\pm 10\%$ .

### HTMSU with integrated conductivity sensor fabrication

A detailed description of the HTMSU fabrication has been given by Adams *et al* with a schematic of the device shown in Figure 1A.<sup>20</sup> Briefly, the HTMSU was hot embossed into PMMA substrates via micro-replication from a metal mold master. The HTMSU consisted of a series of 51 high-aspect ratio curvilinear channels that in concert formed the cell capture bed. Each channel was 150 (depth)  $\times$  30  $\mu\text{m}$  (width) and shared common inlet/outlet ports. Curvilinear-shaped capture channels were used to improve the cell capture efficiency. The cell-free marginal zone apparent in straight channels was not observed in curvilinear channels and the cell radial distribution was unaffected by changes in cell translational velocity. Cells migrate to the outside of the curved channels due to centrifugal forces acting on the cells and the cross-stream velocity component due to the reversal of the direction of curvature.<sup>20</sup> The result is an increase in the aptamer/antigen encounter rate as the cells moved through the capture beds at the relatively high linear velocities used here. The channel width of the cell capture bed (30  $\mu\text{m}$ ) was comparable to the average target cell diameter, which was used to increase the probability of cell:aptamer interactions with the solution-borne target cells. The large channel depth (150  $\mu\text{m}$ ) was selected to reduce the pressure drop in high volume flow rates and also, to increase sample processing throughput.

Appropriately cleaned PMMA HTMSUs devices and cover plates were exposed through a mask to ultraviolet (UV) radiation resulting in the formation of carboxylate moieties only in the exposed areas of the PMMA. The exposed areas were restricted to only the cell capture bed region of the device.<sup>20</sup> UV irradiation was performed through an aluminum mask for 10 min at 15  $\text{mW cm}^{-2}$  to facilitate the formation of the carboxylated scaffold. These parts were then aligned and clamped together between two borosilicate plates. The cover plate was thermally fusion bonded to the substrate by placing the clamped pieces inside a convective oven and heating to  $\sim 101^\circ\text{C}$ , slightly above the glass transition temperature of the UV-modified material. The temperature was increased from  $50^\circ\text{C}$  to  $101^\circ\text{C}$  at a rate of  $20^\circ\text{C}/\text{min}$  and held at  $101^\circ\text{C}$  for 15 min. Polyimide-coated fused silica capillaries were then inserted into the inlet port of the assembled HTMSU to provide introduction of samples into the device using a programmable syringe pump (Harvard, Holliston, MA).

Pt electrodes ( $d = 76 \mu\text{m}$ ) served as the contact conductivity sensor in the detection zone of the HTMSU and were placed into guide channels that were positioned orthogonal to the fluidic output channel following thermal assembly. Insertion of the electrodes was monitored using a microscope to carefully control the inter-electrode gap (50  $\mu\text{m}$ ). The cell constant of the Pt conductivity sensor,  $K$ , was  $\sim 0.01 \mu\text{m}^{-1}$ , which allowed for the specific detection of LNCaP cells based on their average size (diameter = 25  $\mu\text{m}$ ).

### Antibody immobilization to the HTMSU

Antibody immobilization was carried out in a two step process. The UV-modified thermally assembled HTMSU device was loaded with a solution containing 4  $\text{mg/mL}$  EDC, 6  $\text{mg/mL}$  NHS in 150  $\text{mM}$  MES ( $\text{pH} = 6$ ) for 1 h at room temperature to obtain the succinimidyl ester intermediate. After this incubation, the EDC/NHS solution was removed by flushing nuclease free  $\text{H}_2\text{O}$  through the device. Then, an aliquot of 1.0  $\text{mg/mL}$  of the monoclonal anti-EpCAM antibody solution contained in 150  $\text{mM}$  PBS ( $\text{pH} = 7.4$ ) was introduced into the HTMSU and allowed to react for 4 h. The device was then rinsed with a solution of PBS ( $\text{pH} = 7.4$ ) to remove any non-specifically bound anti-EpCAM antibodies.

### Aptamer immobilization onto PMMA films and the HTMSU device

A schematic of the aptamer immobilization process is given in Figure 1B. Aptamer immobilization to PMMA surfaces was carried out in a single step. Following PMMA activation using UV light to generate the carboxylic acid functional scaffold, the activated PMMA surfaces were incubated with a solution containing 10  $\mu\text{M}$  of an oligonucleotide with a random sequence or the PSMA aptamer, 4 mg/mL EDC, and 6 mg/mL NHS in 150 mM MES (pH = 6) and allowed to incubate for 3 h at room temperature. For PMMA films, the planar surface was immersed in the reaction solution. Following reaction, the PMMA surface was rinsed with a solution of PBS (pH = 7.4) to remove any non-specifically bound constituents.

In the case of the HTMSUs, the assembled devices were loaded with a 10  $\mu\text{M}$  anti-PSMA aptamer solution also containing 4 mg/ml EDC and 6 mg/mL NHS in 150 mM MES (pH = 6). This solution was allowed to incubate in the device for 2 h at room temperature. The device was then rinsed with a solution of PBS (pH = 7.4) at 20  $\mu\text{L}/\text{min}$  flow rate to remove any non-specifically bound constituents.

### Determination of aptamer surface density on UV-modified PMMA

A clean SPR gold sensor surface was coated with 300  $\mu\text{L}$  of a PMMA solution (1.0 mg of PMMA in 10  $\mu\text{L}$  of  $\text{CH}_2\text{Cl}_2$ ) in a custom built spin coater and spun at 1,500 rpm for 1 min. The PMMA film was then subjected to UV light and aptamer immobilization was undertaken using identical conditions as those described above. The SPR response, which was measured using a BIACORE X SPR instrument (Piscataway, NJ), was recorded after each treatment using DI water as a buffer. The difference in SPR response before and after aptamer immobilization was determined and the SPR response unit (RU) was converted into molecules/ $\text{cm}^2$  using the manufacturer's conversion factor of 10 RU = 1 ng/ $\text{cm}^2$  and the molecular weight of the aptamer.<sup>30</sup>

### LNCaP cell capture using the HTMSU

To connect the HTMSU to the pump, a luer lock syringe (Hamilton, Reno, NV) was placed on the pump equipped with a luer-to-capillary adapter (Inovaquartz, Phoenix, AZ). This was then attached to the capillary that was sealed to the input port of the HTMSU. A pre-capture rinse was performed with 0.2 mL of 150 mM PBS at 50 mm/s linear velocity to maintain isotonic conditions. Then, the appropriate volume of a cell suspension was introduced at the appropriate volumetric flow rate to produce the desired linear velocity in each microchannel comprising the capture bed. Next, a post-capture rinse was performed with 0.2 mL of 150 mM PBS at 50 mm/s to remove any non-specifically adsorbed cells.

In cases where the cells required optical visualization to assist in the operational optimization of the HTMSU, the PMMA devices were fixed onto a programmable motorized stage of an Axiovert 200M (Carl Zeiss, Thornwood, NY) microscope and video images were collected during each experiment at 30 frames per second (fps) using a monochrome CCD (JAI CV252, San Jose, CA). A Xe arc lamp was used to excite the fluorescent dyes incorporated into the cells' membrane.

### LNCaP cell release from the HTMSU

Following a post cell capture rinse performed with 0.2 ml of 150 mM PBS, a trypsin solution consisting of 0.25% (w/v) trypsin in Tris-Glycine buffer (pH = 7.4) was infused into the HTMSU. The captured cells could be observed (microscopically) until they were removed by the tryptic digestion and Stoke's force using both brightfield video measurements to evaluate release efficiency.

### Conductivity enumeration of released cells

The released cells from the capture surface were traversed at 0.05  $\mu\text{L}/\text{min}$  volume flow rate through a set of Pt electrodes. We used a specially-designed circuit as described earlier<sup>20</sup> to measure the changes in solution conductivity due to single cells as a function of time to create the desired conductivity trace from which cell numbers were determined.

## RESULTS AND DISCUSSION

Although sophisticated imaging reagents and hardware have been developed for the diagnosis and prognosis of many cancer-related diseases, there are still significant advancements that need to be made that can provide earlier diagnosis and staging of cancers following surgical intervention or monitoring disease recurrence.<sup>15</sup> In this work, we exploited the potential utility of CTCs as a diagnostic and prognostic marker for cancer using microfluidics for the high efficiency recovery and subsequent enumeration of prostate tumor cells. The molecular recognition of these cells from clinical samples, such as blood, was enabled by the expression of PSMA into lymph node metastasized LNCaP cells. The selective isolation of these cells directly from whole blood was affected through the use of immobilized anti-PSMA aptamers decorating the walls of a capture bed poised within a HTMSU fabricated in a polymer, which could process large input volumes and search for extremely rare events. The HTMSU contained a conductivity sensor that was used to enumerate the isolated LNCaP cells following chemical release from the capture surface.

### LNCaP cell selectivity and specificity using aptamer recognition

Specific selection of LNCaP cells was based on the recognition capabilities of anti-PSMA aptamers that were tethered to the HTMSU capture beds to select only cells that expressed PSMA even when these cells were of extremely low abundance. The specificity of the PSMA-mediated cell selection by aptamers was investigated by using different surface chemistries, pristine PMMA, UV-modified PMMA, and a capture bed surface decorated with random DNA sequences or PSMA-specific aptamers. These initial experiments used the HTMSU with the adhered cells determined via inspection with fluorescence and brightfield microscopy. In these experiments, the LNCaP cells were seeded into PBS buffer (pH = 7.4) at approximately 1,000 cells/mL and pumped through the HTMSU using a syringe pump (linear velocity = 2.5 mm/s). Because fluorescence microscopy was used for visualization, the cells were fluorescently-stained using a fluorescein membrane probe. From these experiments, we noticed negligible amounts cell adhesion of the LNCaP cells to the channel walls of pristine PMMA. UV irradiation of the polymer modifies the PMMA surface by introducing carboxylic acids and other carbonyl groups onto its surface, making this surface more hydrophilic compared to pristine PMMA.<sup>32</sup> When the LNCaP cell suspension was pumped through this HTMSU device, no LNCaP cells were found to adhere to the UV-modified PMMA surface. Repeating this experiment using a UV-activated PMMA surface that was reacted with 5'-amine containing DNA oligonucleotides possessing a random sequence, no LNCaP cells were detected in the capture bed following fluorescence and brightfield microscopic interrogation. These results suggested that the adhesion forces of the LNCaP cells to these surfaces were not strong enough to withstand the hydrodynamic shear produced by the laminar fluid flow. The random DNA sequences tethered to the PMMA surface did not possess recognition capabilities for the PSMA integral membrane protein. However, when PSMA-specific aptamers were tethered to the capture bed walls, microscopic inspection of the capture beds clearly indicated the presence of captured LNCaP cells (see Figure 2A).

## Cell translational velocity optimization

Because the capture aptamers are tethered to the channel walls, dynamic interactions between the cell membrane's receptors and the channel wall containing the recognition elements is important in determining the recovery of the rare cells. Chang's model<sup>33</sup> of cell adhesion in flowing systems has been applied in previous reports to describe the encounter rate between the solution-borne cells and the surface-tethered cell selection elements.<sup>20</sup> When the flow velocity is beyond an optimal value, a decrease in the interaction time between a particular cell's membrane antigen and the capture molecule available for binding is observed, thereby reducing the number of potential binding events. This model also predicts that too small of a velocity leads to a decrease in the encounter rate between the cell bound antigen and the immobilized recognition element. Therefore, an optimal linear velocity would be expected for each flowing system to guarantee the highest frequency of binding between capture molecules and antigen based on a balance between the interaction time and the encounter rate.<sup>33</sup> In addition, because the solution is driven hydrodynamically through the capture bed, shear force can cause release of the captured cells if the shear force is greater than the adhesion force, which in this case is determined by the PSMA/aptamer dissociation constant and the number of molecular association complexes between the surface and cell.<sup>29</sup>

We therefore carried out experiments to determine the optimal linear velocity to provide the maximum recovery of rare tumor cells found in peripheral blood using aptamer recognition elements. The results of these investigations are presented in Figure 2B. From these results, the maximum cell capture efficiency was found to occur at a translational velocity equal to 2.5 mm/s under the conditions employed in this study. LNCaP cell capture studies using an EpCAM antibody tethered HTMSU followed the same capture efficiency trend for that observed for the anti-PSMA aptamer, indicating that the cell capture efficiency is governed by the same principal as that described by the Chang model and seen in our previous work for anti-EpCAM captured MCF-7 cells using this HTMSU.<sup>20</sup> However, the optimum linear cell translational velocity for maximum cell capture for the anti-EpCAM immobilized HTMSU was slightly lower (2.0 mm/s) than that observed for the anti-PSMA aptamer (2.5 mm/s) indicating that the reaction rate for the anti-EpCAM/EpCAM interaction is slightly less than that observed for the anti-PSMA aptamer/PSMA interaction. The molecular weight of EpCAM, 33 kDa,<sup>34</sup> is far less compared to 100 kDa for PSMA.<sup>16</sup> The extracellular domain of EpCAM contains only 242 amino acid residues whereas PSMA contains 707 extracellular amino acid residues potentially giving extended accessibility of the extracellular domain of PSMA to its recognition element. However, the rate of association will depend also on the location of the recognition epitope as well as the conformational reorganization occurring during a binding event. These factors may provide a faster rate of reaction observed in the case of the anti-PSMA aptamer/PSMA complex. In addition, the expression level of PSMA ( $1 \times 10^6$  molecules/cell) is approximately twice the expression level of EpCAM within the LNCaP cell's membrane.<sup>35-37</sup> This higher expression level and the bulky extracellular domain of PSMA may hinder accessibility of anti-EpCAM/EpCAM interactions due to molecular crowding effects. Moreover, the smaller molecular weight anti-PSMA aptamer, 10 kDa, is able to efficiently bind to the larger molecular weight PSMA due to its capability to quickly fold into thermodynamically stable secondary and tertiary structures to form complexes through molecular forces that specify target interaction.<sup>38</sup>

Another issue that must be addressed is the adhesion strength between the captured cell and its surface immobilized recognition element due to the fact that the shear force exerted by the solution can potentially dislodge the cell from the capture surface. This would occur if the adhesion strength (or force) is less than the shear force ( $F_S$ ). The adhesion force ( $F_A$ ) between the cell and the anti-PSMA aptamer decorated surface can be determined from the

bond strength between a single antigen:aptamer complex ( $f_C$ ), the cell contact area with the PMMA surface ( $A_C$ ) and the number of receptors poised on the PMMA surface within the contact area of the cell ( $C_S$ ) from:<sup>20</sup>

$$F_A = f_C \times A_C \times C_S \quad (1)$$

If the cell is assumed to be a non-deformable object upon adhesion to the capture surface, the contact area can be calculated using;<sup>39</sup>

$$A_C = \pi(r \sin(\cos^{-1}(r - h' + h)/r))^2 \quad (2)$$

where  $r$  is the cell radius and  $h$  and  $h'$  represent the characteristic cell separation distances from the surface upon binding. Using  $h$  and  $h'$  as 100 Å and 400 Å, respectively,<sup>40</sup> the calculated contact area was determined to be 1.88  $\mu\text{m}^2$  for the LNCaP cells ( $r = 12.5 \mu\text{m}$ ). If the cell is assumed to flatten and elongate after contact, as observed experimentally (see Figures 2 and 3), the resulting contact area  $A_C$  was calculated to be approximately 380  $\mu\text{m}^2$ .<sup>41</sup>

The single PSMA:anti-PSMA aptamer adhesion force was estimated using the formalism by Bell,<sup>42</sup> who developed the following expression for deriving the critical force required to break a single bond;

$$f_C = kT/r_o\alpha_C \quad (3)$$

where  $k$  is Boltzman's constant,  $T$  is the absolute temperature,  $r_o$  is the separation distance between receptors at the minimum breaking force and  $\alpha_C = KC_S$  ( $K = \text{PSMA:anti-PSMA}$  aptamer equilibrium constant). Using a value of  $K = 4.76 \times 10^8 \text{ M}^{-1}$ ,<sup>29</sup> and  $r_o = 0.5 \text{ nm}$ ,<sup>33</sup> the value calculated for the adhesion force per association complex was determined to be  $4.55 \times 10^{-11} \text{ N}$ . For the LNCaP cells shown in Figure 3A,  $F_A$  was calculated to be  $5.5 \times 10^{-5} \text{ N}$ .<sup>41</sup>  $F_S$  was determined from Stokes' law;<sup>43</sup>

$$F_S = 6\pi\eta r v_C \quad (4)$$

where  $r$  is the cell radius ( $\sim 12.5 \mu\text{m}$  for LNCaP cells),<sup>44</sup>  $\eta$  is the solution viscosity (4.8 cP for whole blood with a hematocrit level of 0.4)<sup>45</sup> and  $v_C$  is the critical linear velocity that can induce cell detachment. Rearrangement of equation 4 produced a value of  $6.0 \times 10^3 \text{ cm/s}$  for  $v_C$ . This value is significantly greater than the linear velocities used in the present experiments for optimizing the capture efficiency. Several captured cells were observed continuously during experiments in which linear velocities up to 10.0 cm/s were implemented and no cell damage or disruption of cell:wall adhesion was observed.

### Selection of other CTC types using the HTMSU with immobilized PSMA-aptamers

Non-specific adsorption or recognition of other CTC-types was also evaluated using a breast cancer cell line (MCF-7) as an example, which does not express PSMA but does over-express the epithelial cell adhesion molecule, EpCAM. The existence of PSMA genes in normal and non-prostate specific tumor cells, such as the MCF-7 cell line, has been reported,

however, protein assay results for the MCF-7 cell lines failed to detect the PSMA antigen.<sup>46</sup> Our results indicated that no MCF-7 cells were found in the PMMA capture beds when decorated with the anti-PSMA aptamers as deduced from microscopic interrogation of these beds using brightfield microscopy (data not shown). These cell capture experiments were carried out under dynamic laminar flow conditions in the HTMSU microfluidic channels using the optimized LNCaP linear velocity of 2.5 mm/s. Therefore, the presence of the hydrodynamic shear would most likely detach any non-specifically bound material due to weak adhesion forces exerted on these cells.

### Cell detachment from the capture surfaces

Releasing the cells intact from the capture bed was critical for the subsequent conductivity enumeration of the LNCaP CTCs. The mechanism we evaluated for cell release was the use of enzymatic digestion of the extracellular domain of the PSMA protein using trypsin to reduce the cell's adhesion strength to the aptamer surface. There are two main biosynthetic forms of PSMA within the LNCaP cell membrane, which are either mannose-rich PSMA (PSMA<sub>M</sub>) or the glycosylated form of PSMA (PSMA<sub>C</sub>). PSMA<sub>M</sub> is completely sensitive to trypsin, whereas PSMA<sub>C</sub> is trypsin resistant due to transport blockage at the Golgi complex associated with their secretory pathway.<sup>47</sup>

Introduction of a trypsin solution into the capture bed to allow for tryptic digestion of PSMA to provide release of the captured LNCaP cells was found to effectively release these cells from the aptamer-decorated surface indicating the dominate component was PSMA<sub>M</sub> as the attachment partner between PSMA and the anti-PSMA aptamers. Figure 4A represents time-lapse micrographs of a captured cell that was processed using a trypsin digestion solution. Close investigation of the time-lapse micrographs indicated efficient release of the intact LNCaP cells from the capture surface. The cell releasing efficiency increased with increasing incubation time according to Figure 4B. Complete cell detachment (~100%) was achieved in less than 7 min of incubation time. We also note that brightfield inspection at the Pt electrode pair readout point of the device was performed of the released cells following trypsin processing and these inspections confirmed that the cells were intact at this point.

### Conductivity enumeration of the CTCs

The conductivity detector, which consists of a pair of Pt electrodes with a 50  $\mu\text{m}$  spacing (cell constant =  $0.01 \mu\text{m}^{-1}$ ), was fabricated specifically to transduce the larger CTCs compared to the smaller leukocytes and/or erythrocytes that may appear in the enumeration phases of the assay providing false positive signals due to the universal nature of the conductivity response. Also, the CTCs possess unique electrical properties due to their characteristic chemical composition compared to erythrocytes and leukocytes to provide efficient conductivity readout.<sup>48</sup> For example, the over-expression of membrane glycoproteins, such as PSMA, associated with many tumor or cancer cells result in an increase in the number of negatively charged sialic acid molecules that cap the extracellular domains of these integral membrane proteins.<sup>20</sup> This can produce a cell with a higher electrical conductivity compared to one that does not over-express these types of proteins.

One mL of whole blood was seeded with  $20 \pm 1$  LNCaP cells and was processed using the HTMSU. The captured cells were subsequently released using the trypsin releasing buffer and enumerated with the conductivity transducer with a typical data stream shown in Figure 5A. The conductivity transducer measured changes in the conductivity releasing buffer induced by the presence of single CTCs between the Pt electrode pair. Therefore, the responses generated in the data shown in Figure 5A were generated from single cells. Tris-Glycine buffer was selected as the major component in the release buffer due to its low conductance, hence, the sensitivity of the conductivity detection for single cells was

enhanced and the resultant peaks should exhibit a positive response due to the higher conductance of the LNCaP cells with respect to the release buffer. There were 18 peaks in the conductance response given in Figure 5A that could be assigned to single LNCaP cells based on a signal-to-noise threshold of 3 (99.7% confidence level) giving a recovery of ~90% (see insets to Figure 5A showing the discrimination threshold used). As seen in Figure 5A, only positive signals were designated as LNCaP cells and the negative spikes were assigned to particulates due to their lower conductance compared to the Tris-Glycine buffer. Variation of the peak response for each cell is most likely due to differences in the cells' morphology and chemical composition, which is determined by the state of mitosis of the cell.

One ml of a blank sample, which consisted of whole blood seeded with no LNCaPs cells, was analyzed by the HTMSU and enumeration via conductivity under the same conditions as described for the whole blood sample seeded with LNCaP cells and the resultant trace is shown in Figure 5A. In this case, no single cell spikes were seen in the data trace indicating that the signal spikes seen in the conductivity trace for the LNCaP seeded whole blood was indeed due to these tumor cells. Therefore, the purity of LNCaP cell selection was determined to be 100%.

The HTMSU with conductivity enumeration was further evaluated for the detection of various seed levels of LNCaP cells into whole blood to produce a calibration plot. A range of 10 –250 LNCaP cells per ml of whole blood was evaluated. The best fit linear function to the data plotted in Figure 5B had a slope of 0.990 with an intercept near zero ( $r^2 = 0.9997$ ). Interestingly, even at the lowest LNCaP cell load, the data still fit along this linear function indicating that even at extremely low levels of LNCaP cells found in whole blood, we could still quantitatively analyze these cells using the HTMSU. We should note that for 1 mL of whole blood, approximately  $2.5 \times 10^9$  erythrocytes are present. Therefore, the enrichment factor for this assay can be calculated as  $2.5 \times 10^8$  for the lowest LNCaP cell load investigated. At the 2.5 mm/s employed to provide maximum LNCaP recovery, the processing time for exhaustively processing 1 mL of blood would be ~29 min.

## CONCLUSIONS

The HTMSU described in this manuscript utilized an aptamer-based positive selection approach for the isolation of prostate-specific CTCs (LNCaP) directly from whole blood with subsequent quantification of these rare cells using a non-labeling approach. The compelling advantage of this methodology is that no sample pre-treatment was necessary and the throughput (29 min processing time for 1 mL input), recovery (90%) and purity (100%) were extremely high, contrary to what is seen in other rare cell selection formats utilizing size or affinity capture. The ability to quantify the selected cells with near 100% detection efficiency using a conductivity readout format allows for the use of this simple system at the point-of-care for the management of cancer-related diseases from a simple blood test. In addition, molecular profiling of the selected CTCs could be used for determining therapeutic treatment regimens as well as identifying the organ of origin of the selected CTC from whole blood. Molecular profiling of rare CTCs in whole blood could not be done directly on the clinical sample due to the low copy number of the mutated DNA originating from the CTCs as well as potential interferences on downstream molecular processing by the highly abundant red and white blood cells found in whole blood. We are currently in the process of developing sensitive genotyping assays that can be performed directly on the selected CTCs for providing this valuable clinical information.

In our previous report,<sup>20</sup> we performed a positive selection of MCF-7 breast cancer cells from peripheral blood using anti-EpCAM antibodies and this HTMSU. In this report,

aptamers were used for the positive cell selection, in this case for selecting LNCaP cells from peripheral blood. The recovery, purity, and throughput were similar in both cases as well as the specificity for the target cells. The attractive features of aptamers compared to antibodies is the ordered nature of their attachment to the solid surface (5' end attachment) as opposed to a stochastic one associated with antibodies (primary amine groups on the antibody), the ability to carefully control the aptamer/surface distance to improve accessibility and the robust nature of the molecular recognition elements. For example, aptamers can be stored at room temperature without degrading their recognition performance, whereas antibodies must be stored in more controlled conditions to maintain their activity.

## Acknowledgments

We would like to thank the National Institutes of Health (National Cancer Institute, 1 R33 CA099246-01) for supporting this work. This work was also supported in part by the National Science Foundation under Grant Number EPS-0346411 and the State of Louisiana Board of Regents Support Fund. We also thank Dr. Robert Truax from the Louisiana State University School Veterinary Medicine for culturing cells and Dr. Proyag Datta from the Louisiana State University – Center for Advanced Micro-Devices – for replicating the microfluidic devices.

## Abbreviations

<b>PSMA</b>	prostate specific membrane antigen
<b>HTMSU</b>	high throughput micro-sampling unit
<b>PSA</b>	prostate specific antigen
<b>CTCs</b>	circulating tumor cells
<b>LNCaP</b>	lymph node metastasis prostate cancer cells
<b>EpCAM</b>	epithelial cell adhesion molecules
<b>SPR</b>	surface plasmon resonance

## References

1. Serda RE, Adolphi NL, Bisoffi M, Sillerud LO. *Mol Imaging*. 2007; 6:277–288. [PubMed: 17711783]
2. Martin-Orozco RM, Almaraz-Pro C, Rodriguez-Ubrega FJ, Cortes MA, Roper S, Colomer R, Lopez-Ruiz P, Colas B. *Neoplasia*. 2007; 9:614–624. [PubMed: 17898861]
3. Moon C, Park JC, Chae YK, Yun JH, Kim S. *Cancer Lett*. 2008; 266:116–134. [PubMed: 18440696]
4. Loeb S, Catalona William J. *Oncologist*. 2008; 13:299–305. [PubMed: 18378540]
5. Eskew LA, Bare RL, McCullough DL. *J Urology*. 1997; 157:199–202.
6. Rosser CJ, Broberg J, Case D, Eskew LA, McCullough D. *Urology*. 1999; 54:853–856. [PubMed: 10565746]
7. Cristofanilli M, Budd GT, Ellis MJ, Stopeck A, Matera J, Miller MC, Reuben JM, Doyle G, Allard WJ, Terstappen LWMM, Hayes DF. *N Engl J Med*. 2004; 351:781–791. [PubMed: 15317891]
8. Feldstein M, Zelen M. *Breast cancer research and treatment*. 1984; 4:3–10. [PubMed: 6697009]
9. Lin, P.; Ghetti, A.; Shi, W.; Tang, M.; Harvie, GL.; Tao, H.; Tao, G.; Wu, L.; Cerny, D.; Xu, J. Application: US. USA: 2008. p. 38Cont -in-part of U S Ser No 497, 919
10. Logothetis CJ, Navone NM, Lin SH. *Clin Cancer Res*. 2008; 14:1599–1602. [PubMed: 18347159]
11. Nagrath S, Sequist LV, Maheswaran S, Bell DW, Irimia D, Ulkus L, Smith MR, Kwak EL, Digumarthy S, Muzikansky A, Ryan P, Balis UJ, Tompkins RG, Haber DA, Toner M. *Nature*. 2007; 450:1235–1239. [PubMed: 18097410]
12. Hayes DF, Smerage J. *Clin Cancer Res*. 2008; 14:3646–3650. [PubMed: 18559576]

13. Sardana G, Jung K, Stephan C, Diamandis EP. *J Proteome Res.* 2008; 7:3329–3338. [PubMed: 18578523]
14. Schuur ER, Henderson GIA, Kmetec LA, Miller JD, Lamparski HG, Henderson DR. *J Bio Chem.* 1996; 271:7043–51. [PubMed: 8636136]
15. Steeg PS. *Nature Med.* 2006; 12:895–904. [PubMed: 16892035]
16. Silver DA, Pellicer I, Fair WR, Heston WD, Cordon-Cardo C. *Clin Cancer Res.* 1997; 3:81–85. [PubMed: 9815541]
17. Rosenthal SA, Haseman MK, Polascik T. *J Tech Urology.* 2001; 7:27–37.
18. Tasch J, Gong M, Sadelain M, Heston WDW. *Crit Rev Immunol.* 2001; 21:249–261. [PubMed: 11642607]
19. Liu T, Wu LY, Kazak M, Berkman CE. *Prostate.* 2008; 68:955–964. [PubMed: 18361407]
20. Adams AA, Okagbare PI, Feng J, Hupert ML, Patterson D, Gottert J, McCarley RL, Nikitopoulos D, Murphy MC, Soper SA. *J Am Chem Soc.* 2008; 130:8633–8641. [PubMed: 18557614]
21. Dainiak MB, Kumar A, Galaev IY, Mattiasson B. *Adv Biochem Eng/Biotechnol.* 2007; 106:1–18.
22. Liu YJ, Guo SS, Zhang ZL, Huang WH, Baigl D, Xie M, Chen Y, Pang DW. *Electrophoresis.* 2007; 28:4713–4722. [PubMed: 18008303]
23. Diener, JL.; Hatala, P.; Killough, JR.; Wagner-Whyte, J.; Wilson, C.; Zhu, S. Application: WO. Archemix Corp; USA: 2006. p. 207
24. Tombelli S, Minunni M, Mascini M. *Biomol Eng.* 2007; 24:191–200. [PubMed: 17434340]
25. Potyrailo RA, Conrad RC, Ellington AD, Hieftje GM. *Anal Chem.* 1998; 70:3419–3425. [PubMed: 9726167]
26. Balamurugan S, Obubuafo A, Soper SA, Spivak DA. *Anal Bioanal Chem.* 2008; 390:1009–1021. [PubMed: 17891385]
27. Shanguan D, Tang Z, Mallikaratchy P, Xiao Z, Tan W. *Chem BioChem.* 2007; 8:603–606.
28. Vorhies JS, Nemunaitis JJ. *Biologics: Targets & Therapy.* 2007; 1:367–376.
29. Lupold SE, Hicke BJ, Lin Y, Coffey DS. *Cancer Res.* 2002; 62:4029–4033. [PubMed: 12124337]
30. Balamurugan S, Obubuafo A, Soper SA, McCarley RL, Spivak DA. *Anal Chem.* 2008; 80:9630–9634. [PubMed: 18989937]
31. Phillips JA, Xu Y, Xia Z, Fan ZH, Tan W. *Anal Chem.* 2009; 81:1033–1039. [PubMed: 19115856]
32. Witek MA, Wei S, Vaidya B, Adams AA, Zhu L, Stryjewski W, McCarley RL, Soper SA. *Lab Chip.* 2004; 4:464–472. [PubMed: 15472730]
33. Chang KC, Hammer DA. *Biophys J.* 2000; 79:1891–1902. [PubMed: 11023895]
34. Chen YH, Yu T, Bai Y, Zhao N. *Cancer Lett.* 1999; 144:101–105. [PubMed: 10503883]
35. Heston WD. *Urology.* 1997; 49:104–112. [PubMed: 9123729]
36. Balzar M, Winter MJ, De Boer CJ, Litvinov SV. *J Mol Med.* 1999; 77:699–712. [PubMed: 10606205]
37. Schmittgen TD, Teske S, Vessella RL, True LD, Zakrajsek BA. *Int J Cancer.* 2003; 107:323–329. [PubMed: 12949815]
38. Jayasena SD. *Clin Chem.* 1999; 45:1628–1650. [PubMed: 10471678]
39. Cozens-Roberts C, Quinn JA, Lauffenburger DA. *Biophys J.* 1990; 58:107–125. [PubMed: 2166596]
40. Clausen, J. *laboratory Techniques in Biochemistry and Molecular Biology.* Vol. 1. 1981. Immunochemical techniques for the identification and estimation of macromolecules.
41. McCarley RL, Vaidya B, Wei S, Smith AF, Patel AB, Feng J, Murphy MC, Soper SA. *J Am Chem Soc.* 2005; 127:842–843. [PubMed: 15656615]
42. Bell, GI. *Science.* Vol. 200. Washington, DC, United States: 1978. p. 618-27.
43. Katkov II, Mazur P. *Cell Biochem Biophys.* 1999; 31:231–245. [PubMed: 10736749]
44. Hong S, Shamik K, Enmon RM, O'Connor KC. *In vitro Cellul Dev Biol Anim.* 2004; 40:262–7.
45. Kameneva MV, Watach MJ, Borovetz HS. *Clin Hemorheol Microcirc.* 1999; 21:357–363. [PubMed: 10711771]

46. Gala JL, Heusterspreute M, Loric S, Hanon F, Tombal B, Van Cangh P, De Nayer P, Philippe M. Clin Chem. 1998; 44:472–481. [PubMed: 9510850]
47. Castelletti D, Alfalah M, Heine M, Hein Z, Schmitte R, Fracasso G, Colombatti M, Naim HY. Biochem J. 2008; 409:149–157. [PubMed: 17935484]
48. Hakomori S. Immun Allergy Clin. 1990; 10:781–802.

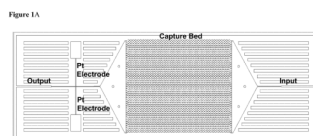
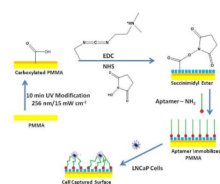


Figure 1B



**Figure 1.** (A) Diagram of the HTMSU made via micro-replication into PMMA from a metal mold master. The capture bed consisted of curvilinear channels that were 30  $\mu\text{m}$  wide and 150  $\mu\text{m}$  deep (51 channels). (B) Process operation of the HTMSU used for the positive selection of LNCaP cells. Also shown is the chemistry used for the immobilization of the cell selection elements, aptamers, to the PMMA surface. The first step involved the UV-irradiation (15  $\text{mW cm}^{-2}$ ) of PMMA and in this case, the irradiation was carried out on just the capture bed so that positive cell selection occurred only in this region.

Figure 2A

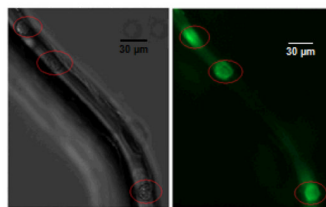
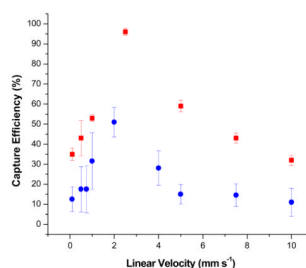
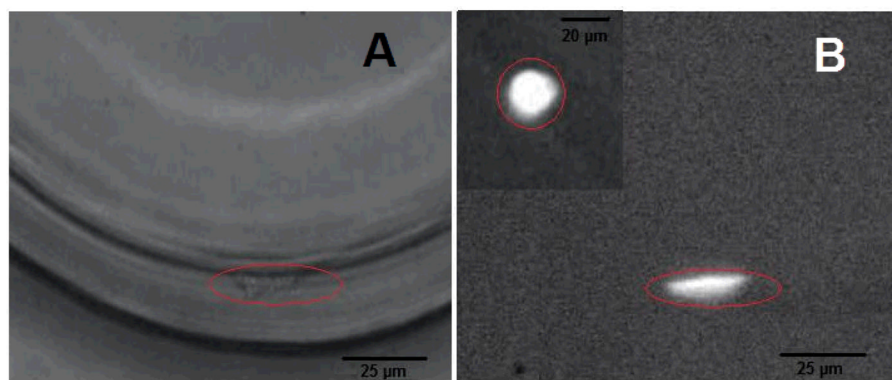


Figure 2B

**Figure 2.**

(A) Brightfield (left) and fluorescence (right) images for the positive selection of LNCaP cells infused into the HTMSU at a constant volumetric flow rate. The cells were suspended in a PBS buffer (~1,000 cells/mL) and following infusion of the cell suspension, the device was washed with PBS buffer prior to imaging. In all cases, the entire capture bed was imaged by scanning the microscope stage. The cells were stained with the fluorescein membrane probe prior to introduction into the HTMSU to allow fluorescence visualization. (B) Comparison of LNCaP cell capture efficiencies using anti-PSMA aptamers or anti-EpCAM antibodies cell recognition elements. In both cases, the HTMSU capture bed was modified with UV light to create the functional scaffold for covalent attachment of the antibody or 5'-labeled aptamer. The graph shows the cell capture efficiency versus cells' translational velocity. Red squares and blue circles represent the capture efficiencies for anti-PSMA aptamers and anti-EpCAM antibodies, respectively. In these experiments, approximately 1,000 LNCaP cells were seeded into a PBS buffer (pH = 7.4) with the number of captured cells determined via brightfield microscopy and subsequently verified using fluorescence microscopy.



**Figure 3.** Brightfield and fluorescence micrographs showing anti-PSMA aptamer captured LNCaP cells in a PMMA microchannel. **(A)** Brightfield micrographs taken at 40 $\times$  magnification and **(B)** the corresponding fluorescence micrographs verifying the captured cell is the fluorescently labeled LNCaP cell. The inset shown in panel **(B)** is a fluorescent-stained LNCaP cell in a PMMA microchannel that was not decorated with anti-PSMA aptamers indicating the spherical shape of these cells.

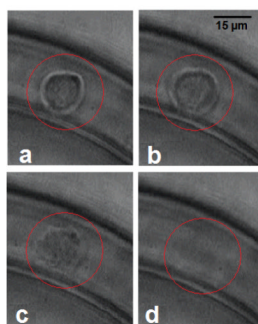
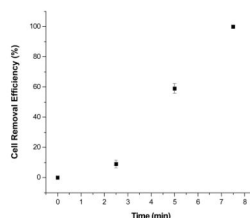
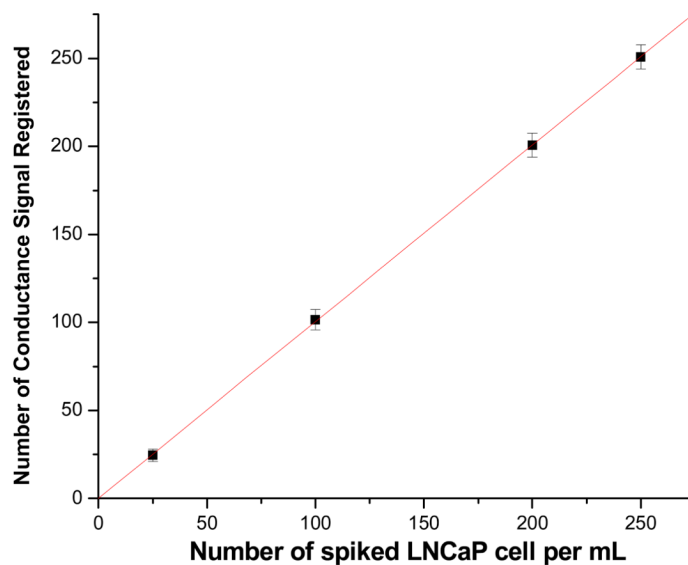


Figure 4B

**Figure 4.**

(A) Time-lapse micrographs showing trypsin enzyme mediated release of a captured LNCaP cell upon application of 0.25% trypsin in PBS buffer (pH = 7.4). (a) At  $t = 0$  or prior to exposure of the captured cells to the trypsin releasing buffer. (b) At  $t = 2.0$  min, disruption of the binding complex is evident. (c) At  $t = 6.5$  min, the cell appears to be released from the capture surface. (d) At  $t = 7.5$  min, the cell was completely released from the surface and swept away from the capture surface to the detection region by the hydrodynamic flow. (B) Plot of cell release efficiency versus time. In each experiment the number of cell releasing events,  $>25$ , in 3 curvilinear channel were counted. The error bars represents the standard deviation of the results obtained for three replicate experiments.

Figure 5B

**Figure 5.**

(A) Conductometric responses generated for 1.0 mL of whole blood seeded with  $20 \pm 1$  LNCaP cells (black) or 0 LNCaP cells (red) at a linear flow velocity of 2.5 mm/s processed using the HTMSU. The captured LNCaP cells were released from the capture surface using the release buffer comprised of 0.25% trypsin and transported through the conductivity sensor at a volumetric flow rate of  $0.05 \mu\text{L}/\text{min}$ . The arrows designate peaks that were identified as LNCaP cells based on a signal-to-noise threshold of 3. The crossed arrows represent non-LNCaP cell events. The insets shown in the figure represent a magnified view of sections of the data stream. The blue line represents the threshold level, which represents  $3\times$  the average background level, that was used to differentiate “true” events from noise. The data presented here was smoothed by the Savitsky-Golay method (25 point smoothing function). Also shown in this plot is a sample of whole blood containing no LNCaP cell that was processed with the HTMSU device (red line). (B) Calibration plot ( $m = 0.990$ ,  $r^2 = 0.99997$ ) for the number of LNCaP cells seeded (10–250 cells/mL) into 1.0 ml of whole blood versus the number of conductivity responses using the Pt-conductivity sensor.